ADVANCED OPTICAL MATERIALS
www.advopticalmat.de

Tattoo-Like Multi-Color Physically Unclonable Functions

N. Burak Kiremitler, Abidin Esidir, Gryphon A. Drake, Ahmet Faruk Yazici, Furkan Sahin, Ilker Torun, Mustafa Kalay, Yusuf Kelestemur, Hilmi Volkan Demir, Moonsub Shim, Evren Mutlugun,* and M. Serdar Onses**

Advanced anti-counterfeiting and authentication approaches are in urgent need of the rapidly digitizing society. Physically unclonable functions (PUFs) attract significant attention as a new-generation security primitive. The challenge is design and generation of multi-color PUFs that can be universally applicable to objects of varied composition, geometry, and rigidity. Herein, tattoo-like multi-color fluorescent PUFs are proposed and demonstrated. Multi-channel optical responses are created by electrospraying of polymers that contain semiconductor nanocrystals with precisely defined photoluminescence. The universality of this approach enables the use of dot and dot-in-rod geometries with unique optical characteristics. The fabricated multi-color PUFs are then transferred to a target object by using a temporary tattoo approach. Digitized keys generated from the red, green and blue fluorescence channels facilitate large encoding capacity and rapid authentication. Feature matching algorithms complement the authentication by direct image comparison, effectively alleviating constraints associated with imaging conditions. The strategy that paves the way for the development of practical, cost-effective, and secure anticounterfeiting systems is presented.

1. Introduction

The widespread consumption of counterfeit products generates substantial economic, social, and health concerns. Conventional ways of preventing counterfeiting involve attachment of security labels to the consumer goods. Watermarks, holograms, graphical barcodes, and security inks are good examples to such security labels. The primary mechanism of protection is the generation of a well-defined response from the security label under a specific challenge. The appearance of a graphical logo under exposure to UV light is a typical example known in banknotes. The main barrier to undesired duplication is the lack of access to techniques and materials used to fabricate the security label. In recent years, the access to information has become extremely easy. As a result, counterfeiters have become proficient in

N. B. Kiremitler, A. Esidir, I. Torun, M. S. Onses
Department of Materials Science and Engineering
Erciyes University
Kayseri 38039, Turkey
E-mail: onses@erciyes.edu.tr

N. B. Kiremitler, A. Esidir, F. Sahin, I. Torun, M. Kalay, M. S. Onses
ERNAM – Erciyes University Nanotechnology Application and Research Center
Kayseri 38039, Turkey

G. A. Drake, I. Torun, M. Shim
Department of Materials Science and Engineering
University of Illinois Urbana–Champaign
Urbana, IL 61801, USA
E-mail: mshim@illinois.edu

A. F. Yazici
Department of Nanotechnology Engineering
Abdullah Gul University
Kayseri 38080, Turkey

F. Sahin
Department of Biomedical Engineering
Faculty of Engineering and Architecture
Beykent University
İstanbul 34398, Turkey

M. Kalay
Department of Electricity and Energy
Kayseri University
Kayseri 38039, Turkey

Y. Kelestemur
Department of Metallurgical and Materials Engineering
Middle East Technical University
Ankara 06800, Turkey

H. V. Demir
Department of Electrical and Electronics Engineering
Department of Physics
Bilkent University
Ankara 06800, Turkey

The ORCID identification number(s) for the author(s) of this article can be found under https://doi.org/10.1002/adom.202302464

DOI: 10.1002/adom.202302464

duplicating security labels. To address this problem, physical unclonable function (PUF) is a promising solution that has recently received significant attention in the scientific community. The response to a challenge is defined by a stochastic process in PUFs. This stochasticity generates an entropic barrier for the duplication of the security label. PUFs have sparked interest in exploiting unique responses of a variety of stochastic processes.[1–3] The randomness in the spatial position, together with the unique properties of materials, have been the most explored strategy in recent studies.

Optical properties of materials exhibit remarkable suitability for constructing PUF systems. The rapid and simple read-out makes optical PUFs highly desirable, and fluorescent materials, in particular, have attracted great attention. The unique excitation and emission wavelengths together with the other characteristics, e.g., fluorescence lifetime, offer a variety of options in the design and manufacture of unclonable surfaces. PUFs based on organic semiconductors,[4–6] photonic polymeric nanospheres,[7,8] metal nanodisks,[9] carbon dots,[10,11] lanthanide-doped zeolites,[12] organic molecules,[13–16] genetically engineered silk,[17,18] and semiconductor nanocrystals[19–27] have been reported recently. Colloidal semiconductors are especially appealing because their optical response is determined by quantum confinement and can be fine-tuned with modulation of their composition and size. Fluorescent PUFs have been developed by ink-jet printing of quantum dots on surfaces with stochastic pinning points.[20–23] Highlighted by these studies, semiconductor nanocrystals are suitable materials for fabricating PUFs. Practical PUF applications require the ability to directly deposit multiple semiconductor nanocrystals over large surfaces with spatial positions determined in a stochastic process. This process should also not involve expensive, time-consuming, or sophisticated methods. A demanding characteristic is the ability to transfer such PUFs on objects of varying composition, geometry and flexibility.

Herein, we propose and show tattoo-like PUFs based on stochastic processing of multi-color semiconductor nanocrystals. The direct, low-cost and stochastic deposition of multiple emitters is enabled by electrospraying. The electrohydrodynamic instabilities inherent to electrospraying provides unpredictability in the position and size of features.[28] However, the polymeric materials commonly used in the electrospraying process lack the unique fluorescence properties that is necessary to construct multicolor PUFs with high-encoding capacity. This concern is overcome by using green-, red-, and blue-emitting semiconductor nanocrystals in dot and dot-in-rod geometries. The additive nature of electrospraying allows direct deposition of these materials on the same substrates, which facilitates multi-color PUFs. The applicability is significantly expanded by using a tattoo-approach, where PUFs electrosprayed on a temporary tattoo paper are transferred to an object of interest. This practical approach decouples the fabrication process from the applied object, thereby greatly relaxing constraints in applications. The structural and photophysical properties of the materials are characterized in detail. To create and authenticate multispectral PUF keys that respond to different excitation channels with high stability without compromising the photophysical properties of quantum dots, we take advantage of the optical and physical properties of the poly(methyl methacrylate) (PMMA) and tattoo paper. Feature extraction algorithms are effectively utilized for authentication. Fluorescence images obtained from multiple channels using a handheld microscope are used to generate digitized keys for rapid authentication. The proposed tattoo-like multi-color PUFs exhibit high-level of stability facilitated by the polymer matrix and semiconductor nanocrystals.

2. Results and Discussion

A schematic representation of our strategy to tattoo-like multicolor PUFs is given in **Figure 1**. There are two main steps in the fabrication. In the first step, multiple fluorescent semiconductor nanocrystals are electrosprayed on a temporary tattoo paper (Figure 1a). The electrospraying is performed from a mixture of PMMA and fluorescent semiconductor nanocrystals dispersed in chloroform. Red, green, and blue-emitting semiconductor nanocrystals were composed of CdSe/CdS dot-in-rods (R-DiRs), CdSe/ZnS QDs (G-QDs), and CdZnS/ZnS QDs (B-QDs), respectively. These semiconductor nanocrystals were selected based on their distinct photoluminescence spectra centered at three different wavelengths, which can be easily distinguished in conventional or handheld fluorescence microscopes.

Here the electrohydrodynamic instability ensures random positioning of the photoluminescent materials. The electric charge carriers are accumulated at the solution's apex when an electric field is applied between the needle and collector in excess of a critical value.[29] The surface tension of the solution is then overcome by the electrical forces, releasing a thin electrically charged liquid jet. As a result of Rayleigh instability, this jet disintegrates into droplets.[30–32] The charged droplets self-disperse due to the Coulombic repulsion force acting on them, in addition to the intricate interplay between drag and gravity. The electrohydrodynamic instability and the droplets' chaotic pathways are primarily responsible for the randomness in the position, size, and morphology of features.[28,31,33,34] These characteristics together with the distinct photophysical properties of fluorescent semiconductor nanocrystals make the surface unclonable.

In the second step, the unclonable surface features are transferred to a target object using a tattoo-approach. For this purpose, red, green, and blue-emitting semiconductor nanocrystals are directly deposited on the tattoo-paper. This kind of paper substrates are used to generate temporary tattoos and have also been

H. V. Demir
LUMINOUS! Center of Excellence for Semiconductor Lighting and Displays
School of Electrical and Electronic Engineering
School of Physical and Mathematical Sciences
and School of Materials Science and Engineering
Singapore 639798, Singapore
H. V. Demir, E. Mutlugun, M. S. Onses
UNAM—Institute of Materials Science and Nanotechnology
Bilkent University
Ankara 06800, Turkey
E-mail: evren.mutlugun@agu.edu.tr
E. Mutlugun
Department of Electrical and Electronics Engineering
Abdullah Gul University
Kayseri 38080, Turkey

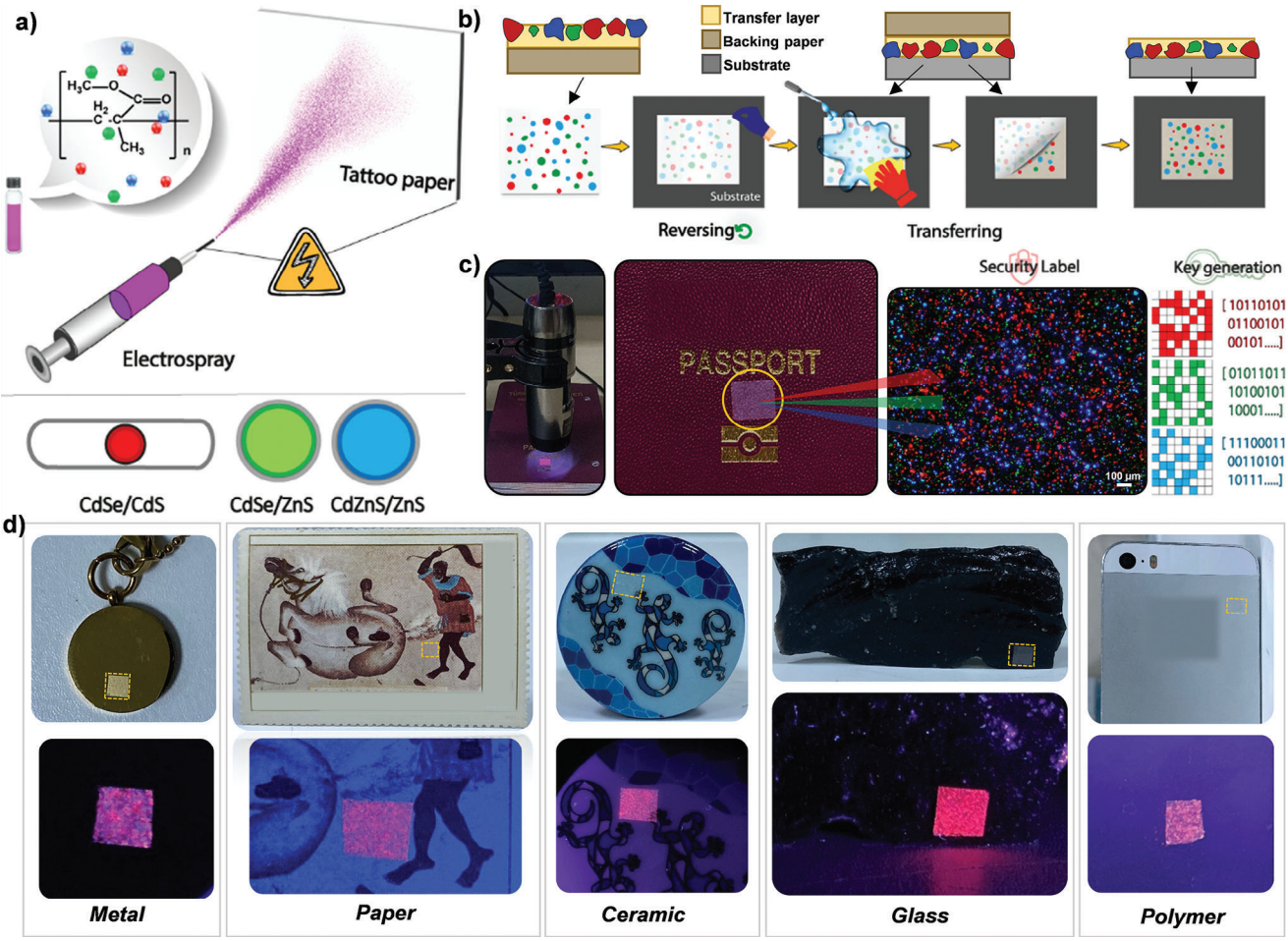

Figure 1. A schematic illustration of the proposed approach for generating tattoo-like multi-color PUFs. a) Electrospraying of fluorescent semiconductor nanocrystals on the tattoo paper. b) Transferring unclonable features via a temporary tattoo paper. c) Demonstration of an application on a passport surface imaging by a handheld fluorescence microscope. Extraction and authentication of multiple PUF keys depending on the emission channels derived from fluorescence images. d) Photographs of PUF labels created on different surfaces such as metal (necklace), paper (antique postage stamp), ceramic (handcrafted brooch), glass (obsidian ore), and polymer (smartphone case).

used to fabricate electronic devices and surface-enhanced Raman scattering-based security labels.[35–37] To the best of our knowledge, this is the first report regarding adaptation of this approach to PUFs. Following the electrospraying of fluorescent nanocrystals, the tattoo paper is faced down on the object of interest. A wet cloth is pressed for about 30 s followed by detachment of the backing paper. This simple process achieves transfer of unclonable features with a thin membrane on the object. As a demonstration, we transferred multi-color PUFs on a passport (Figure 1c). The authentication of the passport, for example, is performed by taking the fluorescence images of the surface features at the level of the manufacturing. These images are used to construct a database of authentic passports. Both digitized keys consisting of binary bits for each color as well as the original images can be used to construct the database. At the point of inspection, a fluorescence image of the passport is taken by a handheld fluorescence microscope and converted to a digitized binary key, which is compared with the one in the database. In a complementary manner, direct authentication of images can be performed by a feature matching algorithm. PUF labels in various sizes and geometries can be readily applied to the surfaces of several objects with diverse surface chemistries and roughness levels thanks to the scalable nature of electrospraying and versatile tattoo transfer technique (Figure 1d).

The semiconductor nanocrystals with distinct peak emission wavelengths were synthesized via colloidal methods. **Figure 2** presents high-resolution TEM images together with absorption and photoluminescence spectra of the used semiconductor nanocrystals. R-DiRs exhibit a uniform rod shape with an average length of 18.9 ± 1.3 nm and a width of 6.0 ± 0.47 nm, whereas G-QDs and B-QDs are spherical with an average diameter of 6.8 ± 1.04 and 6.2 ± 0.97 nm, respectively. R-DiRs, G-QDs, and B-QDs exhibit peak emission wavelengths of 632, 522, and 429 nm along with photoluminescence quantum yields (PLQY) of 90.0%, 60.9%, and 52.9%, respectively. From the PL spectra, the full-width-at-half-maximum (FWHM) values are 35 and 33 nm for B-QDs and G-QDs, respectively, whereas it is a narrower 29 nm for R-DiRs. Axial strain mapping showed that the CdSe core is centrally located along the rod for the R-CdSe/CdS DiRs. (Figure S1, Supporting Information).

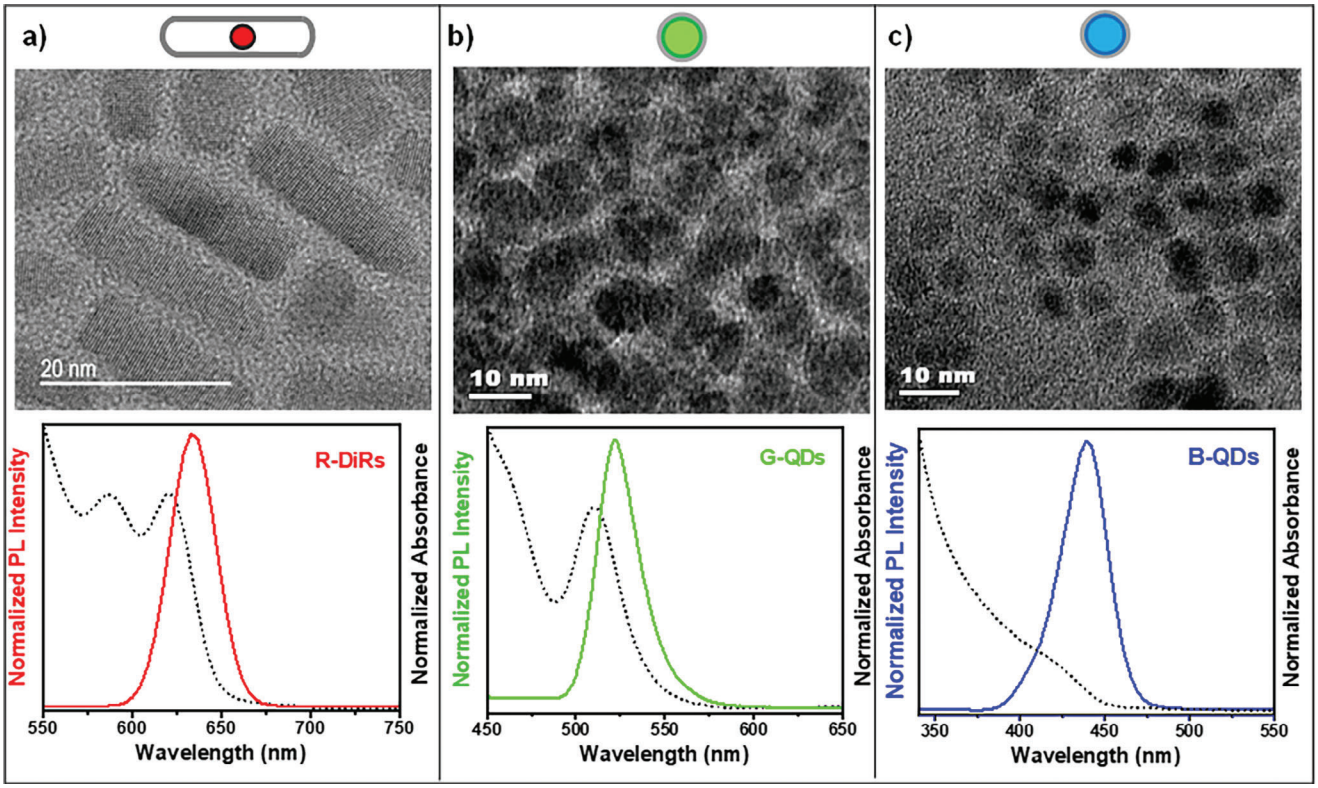

Figure 2. Characterization of fluorescent semiconductor nanocrystals used to construct tattoo-like multi-color PUFs. The HRTEM images, photoluminescence and UV–vis absorption spectra of a) R-DiRs, b) G-QDs and c) B-QDs.

Randomly positioned fluorescent features were generated by electrospraying semiconductor nanocrystals dispersed in a PMMA solution of chloroform. **Figure 3** presents morphology and photoluminescence spectra of the surfaces prepared by electrospraying individual semiconductor nanocrystals yielding monochromatic PUFs. PMMA was chosen due to near-full transparency throughout a broad spectrum of the electromagnetic radiation and very low parasitic absorption.[38] Accordingly, the peak emission wavelengths (632, 523 and 429 nm) measured from PMMA features containing R-DiRs, G-QDs, and B-QDs (Figure 2a–c) did not shift when compared to the colloidal solutions of the semiconductor nanocrystals. The morphology of the electrosprayed features is highly dependent on the properties of the solvent (dielectric constant, conductivity, surface tension, and volatility) and the polymer (concentration, molecular weight, and interaction parameters between the polymer and the solvent).[28,31] Chloroform is an intermediate solvent for PMMA with a Hansen space parameter (Ra) of 7.78 $MPa^{0.5}$, enabling the formation of large features that are easy to observe and identify with fluorescence imaging as shown in Figure 3. Note that electrospraying parameters are chosen to operate in only-bead regime. The mechanical characteristics of the initial droplet permits excessive Coulombic fission tendency, which may have produced progeny droplets. In another related aspect, distinctive wrinkled structures have formed due to a developed mechanical mismatch between the inside and outside of the precursor droplet during the electrospraying process. Wrinkles can be employed as an additional component in physical cryptography due to their strong dynamic light scattering and distinguishing shape.[39–42] Additionally, depending on the type of semiconductor nanocrystals used, the average size of the features may differ. Under identical conditions, PMMA with R-DiRs and B-QDs resulted in features with average sizes of 6.48 ± 1.55 and 6.24 ± 2.22 μm, whereas the features with G-QDs have an average size of 3.39 ± 0.8 μm (Figure S2, Supporting Information).

Sequential electrospraying offers a promising method for fabricating PMMA structures containing multiple quantum nanocrystals that exhibit distinct chemical and spectral properties on a single surface, as illustrated in Figure 3d. Because of electrical charges, these features may indeed be localized not only during the flight, but also in a distinct arrangement on the surface, without overlapping one another due to the repulsion between structures. These features are effectively transferred using the tattoo paper with little to no disruption (Figure S3, Supporting Information).

Figure 4 illustrates our approach for implementing PUF primitives with varying levels of security by leveraging multispectral/color features created using consecutive electrospraying on the same surface. Thirty unique tattoo-like multi-color PUFs were generated on tattoo paper using electrospraying and subsequently transferred onto a silicon surface, as exemplified by sample S29 in Figure 4a. Cryptographic keys were then extracted from each of these features. Figure 4b provides a detailed flowchart outlining the process of extracting cryptographic keys for the response to a specific challenge. Typically, three challenge-response pairs were employed based on the peak wavelengths of the

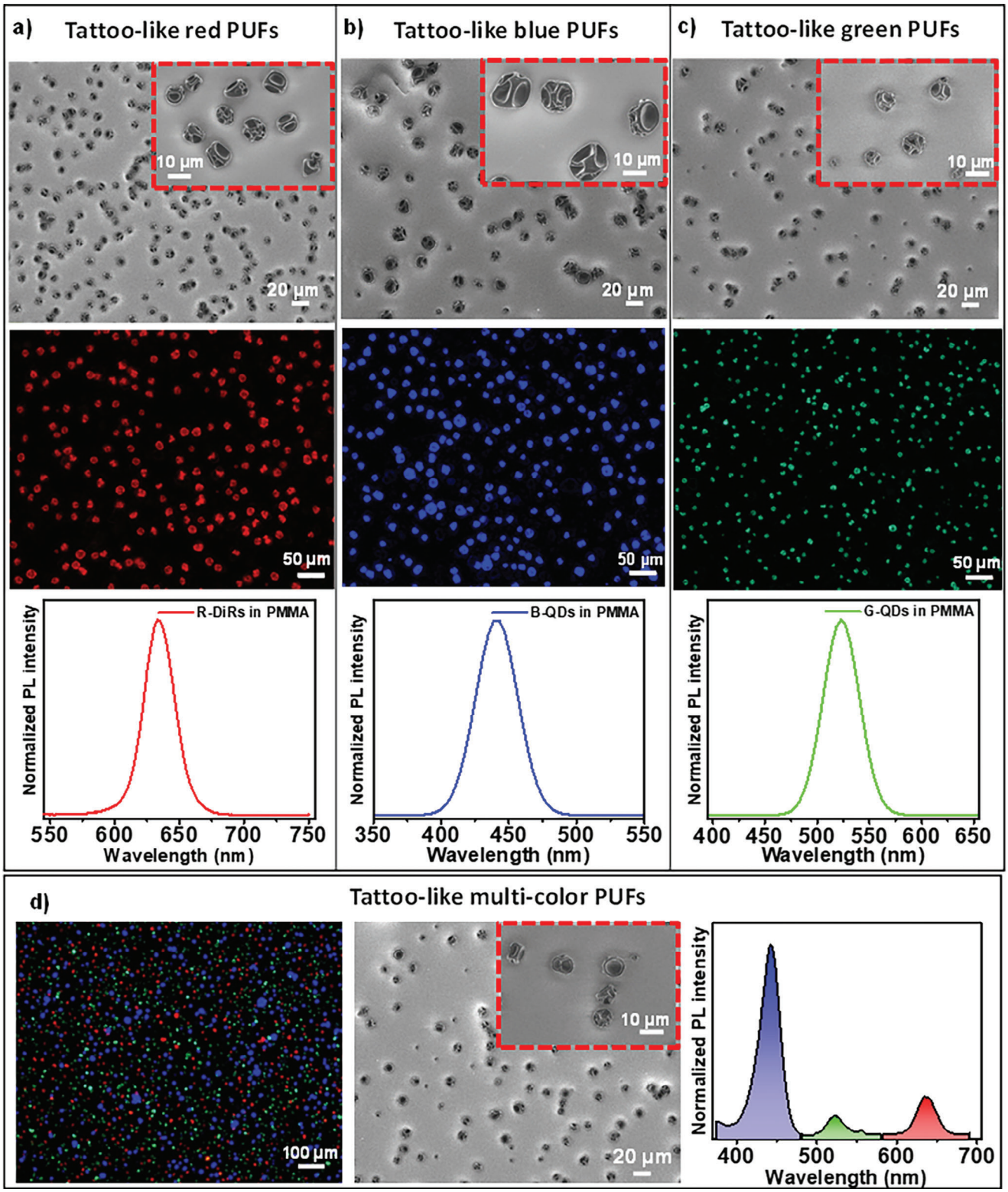

Figure 3. Characterization of the electrosprayed fluorescent features. FESEM images, fluorescence microscopy images and photoluminescence spectra of tattoo-like PUFs: a) red, b) blue, c) green, and d) multicolor tattoo-like PUFs.

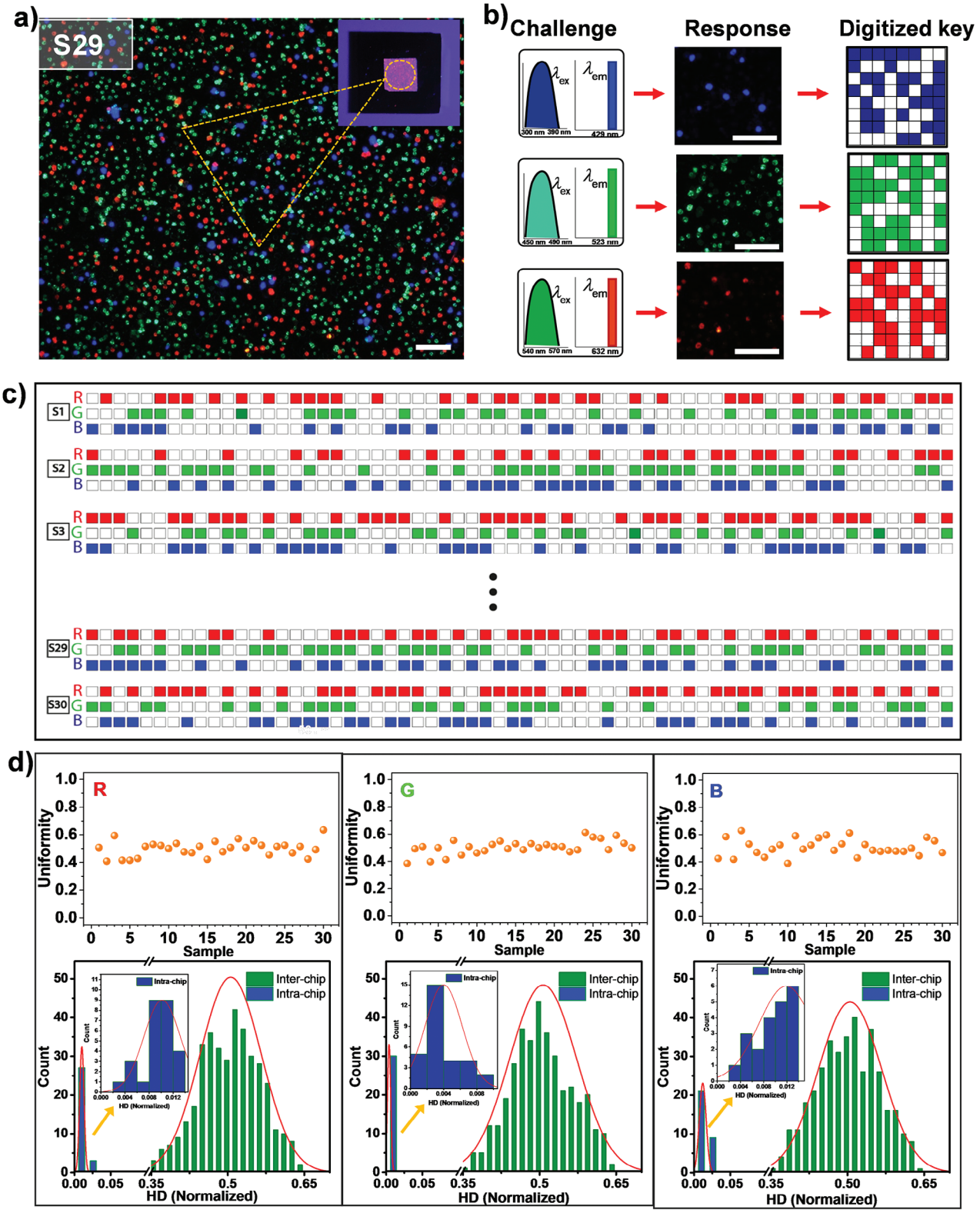

Figure 4. Performance analysis of tattoo-like multi-color PUF: a) Merged fluorescence image as a tattoo-like multicolor PUF with challenge-response dependent components. b) Demonstration of three distinct challenge-response pairings optimized for each of the components that form a single PUF and the unique PUF keys generated from this pairing. Scale bars are 100 μm. c) Examples of 192-bits long unique security keys generated from different samples. d) Analysis of the performance of security keys extracted from each independent subchannel of tattoo-like multi-color PUFs. HD_{INTRA} and HD_{INTER} distribution and uniformity of bit values for each of the three distinct color PUFs for 30 samples.

individual semiconductor nanocrystals present in the tattoo-like multi-color PUFs. The challenges were defined by the excitation wavelength bands of fluorescence filter sets that do not interfere with each other for the respective semiconductor nanocrystals. The filter sets of fluorescence microscope with the emission wavelengths of 540 ± 25, 470 ± 20, and 365 ± 25 nm were used for imaging R-DiRs, G-QDs, and B-QDs, respectively. The corresponding fluorescent images acquired from the individual tattoo-like multicolor-PUFs in response to these distinct optical excitations serve as the output responses. Therefore, a single tattoo-like multi-color PUF can produce three distinct fluorescence images, each displaying its component feature in a unique delocalization and set of colors. This allows for the extraction of multiple cryptographic keys from a single PUF using the corresponding fluorescence images or a merged version of them, enabling the creation of multiple security levels. The extraction processes of individual digitized PUF keys are described in the Supplementary Information and Table S1 (Supporting Information). Each of these binarized and downsized images, based on the color channels, is then utilized to generate 64 (8 × 8) bit or 256 (16 × 16) bit long security keys comprising of 1-bits and 0-bits, as depicted in Figure 4b. Ultimately, we obtained 64- or 256 -bit PUF keys by converting the original images into binary keys. The initial responses of physical systems can exhibit nonuniformity, with the extent of this imbalance dependent on the inherent characteristics of the process. This imbalance primarily stems from using each of the different-colored features as security layers. Creating a multicolored PUF requires each color layer to occupy a fraction of the surface, leading to a relatively low amount of features in fluorescence images compared to the background. As a result, keys generated from single color images have a slightly higher proportion of 1-bits over 0-bits. To tackle this issue, we employed classic von Neumann debiasing during the key extraction process. After implementing this debiasing technique, uniformity of keys improved significantly. In the binarized images, PMMA microparticles decorated with semiconductor nanocrystals appear as colored pixels (0-bits), while the underlying substrate is represented by white pixels (1-bits). Digitizing a single tattoo-like multi-color PUF key involves combining three sets of challenge-response data, each of which could be used as individual PUFs (Figure 4c). The total combination of these PUFs results in a final key size of 192 bits (3 × 64 bits). To assess PUF performance, this process was repeated for 30 individual tattoo-like multi-color PUFs, resulting in 30 unique security keys, each 192 bits long (Figure 4c). For a complete list of the generated keys, please refer to Figure S4 (Supporting Information).

To evaluate the effectiveness of multi-colored features, which consist of three emission channel-specific subkeys, we conducted a thorough analysis of PUF performance.[43] Figure 4d presents analysis of 30 distinct tattoo-like multi-color PUFs based on their respective subkeys. Uniformity, indicates the balanced distribution of 1-bits and 0-bits.[17,43] The average uniformity values for the red, green, and blue subkeys were 0.499 ± 0.055, 0.504 ± 0.052, and 0.507 ± 0.062, respectively. These results are very close to the ideal value of 0.5, suggesting an equal distribution of 0-bits and 1-bits across the keys.

Randomness, another crucial metric that is closely related to uniformity and signifies the stochastic distribution of features, was calculated using the statistical method reported by the National Institute of Standards and Technology (NIST).[44] To verify the randomness, seven different NIST statistical tests were conducted using 60 sequences, each containing 128 bits. These sequences were obtained from a total of 30 different 256 bit long sequences of each PUF subkey, resulting in a collection of 7680 bits for testing purposes. The *p*-values are greater than 0.01, and therefore generated bitstreams of the red, green, and blue subkeys have successfully passed all the randomness tests (Table S2, Supporting Information). We concluded PUF performance analysis by determining the merits of uniqueness and reliability. Uniqueness, which measures a PUF's ability to differentiate itself from other PUFs, was evaluated using the Hamming distance metric.[44] In an ideal case, keys generated from any two particular PUFs should not be correlated. Reliability, on the other hand, is a measurement of the repeatability of responses returned from a PUF when challenged under various conditions. We calculated intrachip (HD_{INTRA}) and interchip (HD_{INTER}) Hamming distance values for each of the subkeys as given in Figure 4d. The HD_{INTER} values were found to follow Gaussian distributions centered at 0.506, 0.507, and 0.505 with standard deviations of 0.060, 0.066, and 0.062 for the red, green, and blue emitting subkeys. These results are in close agreement with the ideal value of 0.5, indicating excellent uniqueness across all subkey groups. The HD_{INTRA} values, which were also calculated, were very close to the ideal value of 0, with an average of 0.00102, 0.00408, and 0.01186 for the red, green, and blue PUF subkeys, respectively. Furthermore, we calculated false positive and false negative rates, accounting for both interdevice and intradevice variabilities. The determination of the cut-off threshold and the subsequent calculation of false positive and false negative rates were carried out by applying the mean and standard deviation to the Gaussian distribution function depicted in Figure 4d. The results are presented in **Table 1**.

Table 1. False Positive/Negative Rates and Cut-off Threshold of Tattoo-Like Multi-Color PUFs.

	Red	Green	Blue
False positive rate	3.10×10^{-16}	1.10×10^{-16}	2.59×10^{-16}
False negative rate	6.64×10^{-20}	6.61×10^{-20}	6.66×10^{-20}
Cut-off threshold	0.1108	0.2219	0.1283

The value of HD_{INTER} is an important parameter in determining the encoding capacity. In this context, the encoding capacity refers to the number of responses that can be produced by the PUF, and generally is calculated as c^s, where c represents the number of response (i.e., colors) and s represents the bit size (i.e., pixel size of the image). However, determining the appropriate value of s is essential to ensure accurate calculation of the encoding capacity. Assuming s equals to the total number of pixels in the image can be misleading, since each pixel may not be completely independent. A solution to this issue is only considering independent bit elements through the calculation of degree of freedom" (DoF) = $\mu(1-\mu)\,\sigma^{-2}$, where μ is the mean value and σ is the standard deviation for HD_{INTER}. The DoF of each color subkey of our tattoo-like multicolor-PUFs are ≈69, ≈57, and ≈65 for the red, green, and blue channels, respectively. Consequently, the encoding capacity for our multi-color PUF system amounts to $\approx 4^{95}$ ($c^s = 2^{69} \times 2^{57} \times 2^{65}$).

We implemented a feature detection-based approach for authentication of tattoo-like multi-color PUFs to fully benefit from the randomized electrosprayed patterns with multiple color responses in fluorescence imaging. Unlike the traditional binary key matching method that relies solely on the compliance of reference markers and scaling criteria,[15,16,45,41] this authentication process provides a highly practical and swift way. To ensure the integrity of the authentication process, we initially stored triple-colored fluorescence microscope images of PUF layers. This step was taken to minimize the risk of theft or manipulation through individual image editing. To authenticate an unknown multi-color PUF, we employed the Oriented Fast and Brief (ORB) algorithm, which is a technique for image feature matching. ORB enables scale independent operation and allows rotation, zooming, and zooming-out.[46,47] This algorithm directly compares images taken at different positions, under different magnifications, and with different contrasts from any emission layer of the label with the complex images stored in the database.[28,41,48–50]

Figure 5 provides several application examples of this image matching process. Fluorescence images acquired at the same magnification and position from different time periods of authentic PUFs are readily correlated to their corresponding counterparts in the database, as depicted in Figure 5a. In the comparison images, the matching rate between the features of the strong spots identified by the ORB algorithm and the features in the color space is approximately 86%, 87%, and 85% for the red, green, and blue channels, respectively. Similarly, as demonstrated in Figure 5b, images obtained from each sub-security layer at a higher magnification by using 20× objective are matched with the relevant points in the unified image within the database. This illustrates the effectiveness of the method in scenarios where position and scale invariance are important factors. The animation of the authentication process can be viewed in Supporting Information. On the other hand, as depicted in Figure S5 (Supporting Information), the sparse matching of features for unauthentic PUF tag when subjected to the ORB algorithm indicates its reliability. Another advantage of this algorithm, in comparison to others, is its ability to detect a higher quantity of key points and its lower computational costs, thereby leading to improved recognition performance.[51] In Figures S6 and S7 (Supporting Information), a comparison of the number of key points generated and recognition rates for PUF tags using the SURF, BRISK, and KAZE algorithms establishes that ORB excels in practical authentication of PUF labels. Using a similar approach as depicted in Figure 5c,d, the PUF labels were directly authenticated by employing the ORB algorithm, while considering all color channels together. During the authentication process, a database of security tags was created by randomly selecting multi-colored tags (Figure 5c: *a1–a5*). Users then captured microscope images of the security labels, which inevitably had variations in brightness, contrast, and defects (Figure 5c: *b1–b5*). To ensure the reliability of the tags, the features extracted using the ORB algorithm were used to calculate the ratio between the similarities of the features matching the tags in the database and the images taken by the users. This similarity rate (S) was calculated using the formula: $S = N_m/N_t$.[13,52,53] Here, N_m represents the number of matching features, whereas N_t represents the total number of features. The similarity values for genuine labels (*a1* between *b1–b5*) are depicted in Figure 5c,d, showing S values of 1, 0.96, 0.71, and 0.7 for *b1* (second capture), *b2,3* (captured under different illumination), *b4* (captured under different magnification with an artificial defect), and *b5* (captured under different magnification and rotation), respectively. Conversely, the similarity rate of fake labels (*c1–c5*) compared to the genuine labels (*a1–a5*) is less than 0.007. These results obtained through feature matching analysis provide practical implications. The significant difference in similarity values between genuine and fake labels allows for the determination of a suitable threshold value, ensuring a wide range of authenticity even in images captured under diverse conditions.

Several aspects need to be considered for the practical implementation of PUFs in real-world samples. The rapid and low-cost read-out of the images is highly important. The registration of the sample, acquisition of images, and computational time for authentication all contribute to the total time of read-out. The most time-consuming step involves the placement and registration of the sample under the image acquisition system. The size and rotation independent nature of ORB feature matching algorithm greatly reduces the constraints associated with this step and enables rapid (< 1 min) authentication including registration of the sample, the computational processing time is as short as 90 ms for the ORB algorithm. The authentication via a commercially available handheld fluorescence microscope with a cost on the order of $1000 makes the process affordable for most applications. The progression of the technological readiness levels will further improve the cost and duration of authentication.

The stability is a crucial factor often overlooked in the use of PUF labels in real-world applications. Ideally, a PUF should consist of multiple security layers, each capable of withstanding environmental effects and providing consistent feedback over an extended period. In our study, we conducted several experiments to assess the stability of the fabricated PUF labels, aiming to address this important aspect. **Figure 6** illustrates the results of these stability tests. In the first test, a sample PUF label was exposed to UV light for several hours, and fluorescence images were captured at specific time intervals for visual and quantitative comparison (Figure 6a). Remarkably, even after 8 h of exposure, the PUF remained highly stable, as evidenced by the comparative images and the graph depicting the change in fluorescence intensity over time. The emission intensity remained above 90% of the initial condition, indicating strong stability under UV light exposure.

To further evaluate the stability, we conducted a thermal test on each individual security layer of a fabricated tattoo-like multi-color PUF (Figure 6b). The sample was subjected to a constant temperature of 70 °C for 10 days. By correlating 256-bit security keys generated from fluorescence photos taken at specific time intervals, we constructed a graph illustrating the time-dependent fluorescence intensity. When considering all security layers, the maximum change in the bit sequence was approximately 1.2%, and the maximum decrease in fluorescence intensity was around 15%. These results indicate that the PUF layers maintained their stability even under prolonged exposure to elevated temperatures. In another experiment, we captured 100 fluorescence microscopy images of each security layer from the same location of a tattoo-like multi-color PUF (Figure 6c). Analyzing the data, we found that the maximum degradation in fluorescence intensity after 100 consecutive imaging sessions was less than 8%, highlighting the high read-out stability of the PUF.

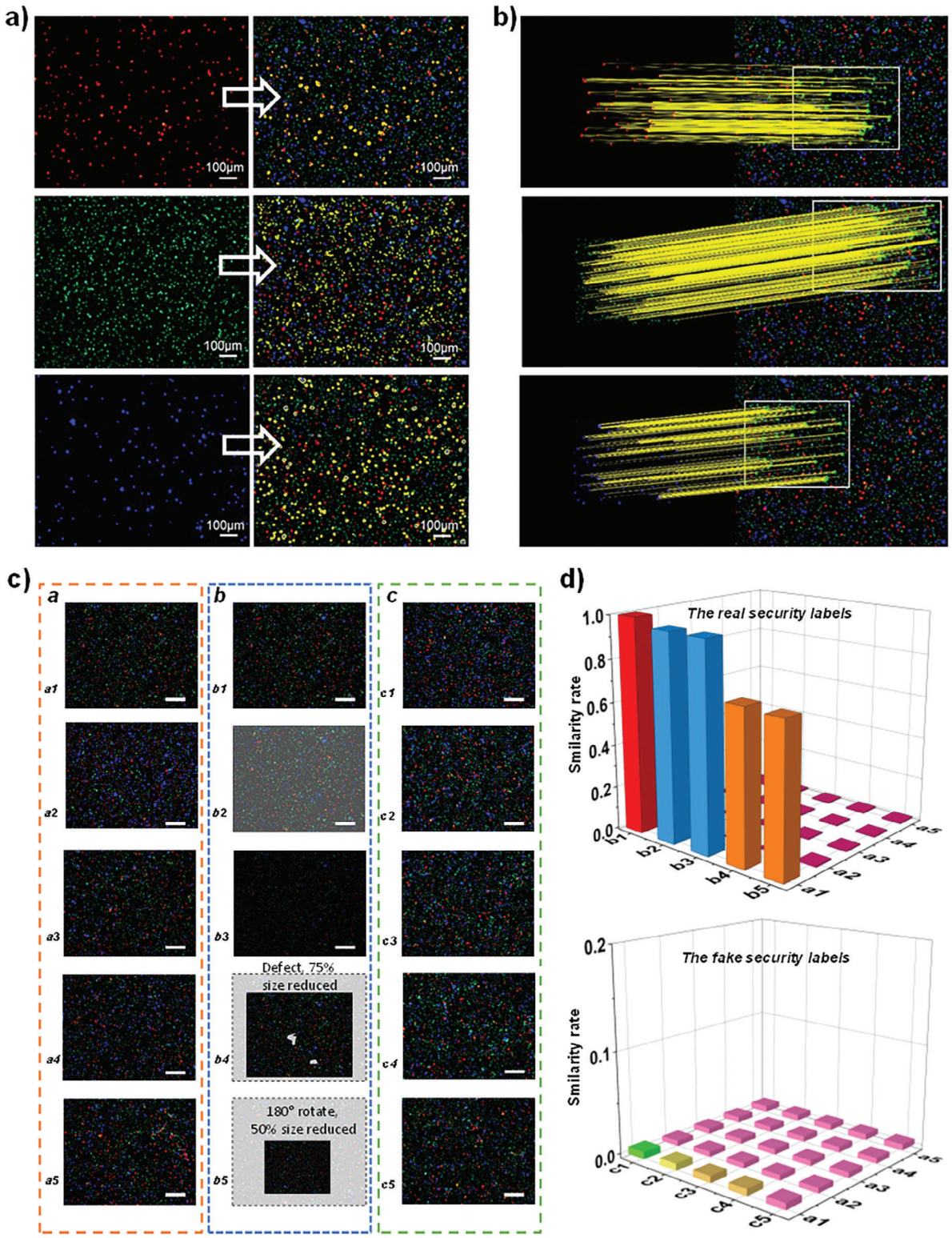

Figure 5. Authentication of tattoo-like multi-color PUFs by feature detection algorithms. a) Matching the multi-layer image stored in the database (right column) with the images of each individual security layer (left column) acquired from the same angle and magnification. Regions that are indicated in yellow are locations with matched points. b) Scale and location invariant authentication of each individual security layers. Green dots are strong feature points that match in both images, and the yellow lines show the positions of these matches. c) *a1–a5*: A database of multichannel images captured from real security labels. *b1–b5*: fluorescence images taken from a real sample (*a1*) under various conditions (*b1*: recapture, *b2,b3*: captured under different illumination, *b4*: captured under different magnification and with an artificial defect, and *b5*: captured under different magnification, and rotation). *c1–c5*: fluorescence images of fake labels. d) Similarity rates given for real labels (*b1–b5*) and fake labels (*c1–c5*). Scale bars are 100 μm.

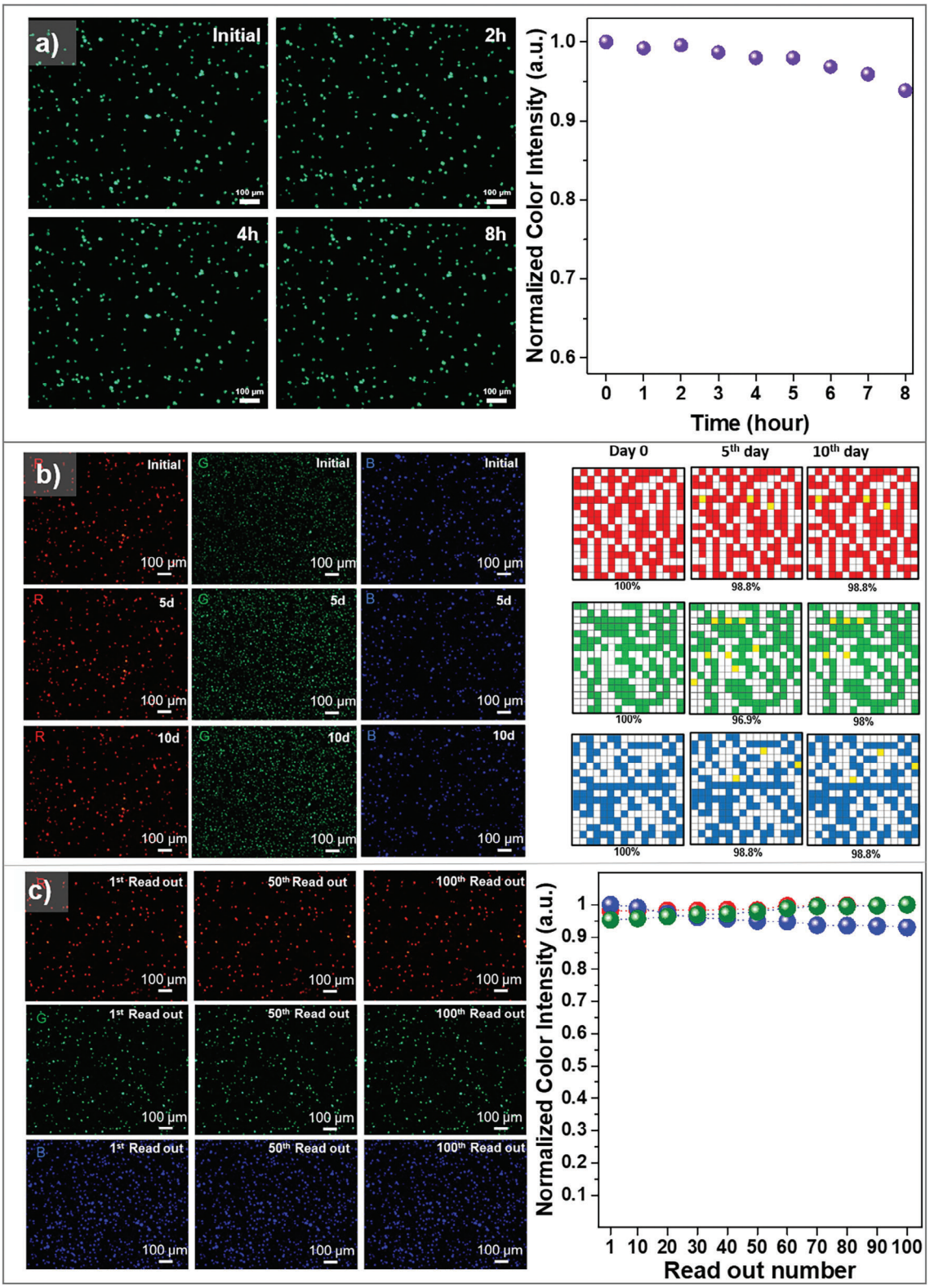

Figure 6. Stability of PUFs. a) UV light stability. Fluorescence images (left) and fluorescence intensity graph (right) as a function of duration of exposure are presented. b) Thermal stability of a tattoo-like multi-color PUFs. Fluorescence images captured from each individual security layer (left), and comparison of extracted keys as a function of heating duration (right). c) Read-out stability. The fluorescence intensity as a function of the number of read-out (right) and comparison of fluorescence microscopy images.

Overall, these findings demonstrate that tattoo-like multi-color PUFs exhibit excellent stability, owing to the use of the electrospraying method to create the PMMA matrix and the thin tattoo transfer membrane that acts as insulation and protection for the semiconductor nanocrystals against external environmental factors. The results emphasize the significance of considering PUF stability in real-world applications, as tattoo-like multi-color PUFs offer accurate and stable identification, enabling multi-layered security in diverse fields.

3. Conclusion

This work has presented tattoo-like multi-color PUFs composed of semiconductor nanocrystals. Leveraging the electrohydrodynamic instability ensures inherent randomness in the position and size of semiconductor nanocrystals, and the additive process enables deposition of multiple materials and high encoding capacity. The unique physicochemical properties of semiconductor nanocrystals pose an additional security barrier for counterfeiters. The key innovation of this work is the ability to transfer unclonable features from the substrate of fabrication to object of interest. This ability decouples the preparation and labeling processes and greatly relaxes constraints in the real-world application. The inherently universal nature of the presented approach enables the adaptability to different types of nanocrystals with unique challenge-response pairs. This adaptability provides design options in accordance with the need of a particular application. Single colored PUFs, for example, will provide a robust solution for modest quantities of products/objects. In demanding applications, multi-color PUFs will ensure enhanced security and tremendously high encoding capacity.

4. Experimental Section

Materials: Cadmium oxide (CdO, ≥99.99%), selenium (Se, ≥99.99%), sulfur (S, ≥99.99%), stearic acid (95%), squalane (95%), trioctylphosphine (TOP, 97%), chloroform (≥99.8%), zinc acetate ($Zn(OAc)_2$, 99.99%), zinc acetate dihydrate ($Zn(OAc)_2$•$2H_2O$, 99.999%), oleic acid (OA, 90%), 1-octadecene (ODE, 90%), acetone, n-hexane, and PMMA (120,000 g/mol) were purchased from Sigma–Aldrich. Octadecylphosphonic Acid (ODPA) and hexylphosphonic acid (HPA) were purchased from PCI Synthesis. Stock solutions of 2 M TOP-Se and TOP-S were formed by dissolving the solid precursors in TOP by stirring in vials inside a glovebox. More dilute TOP–Se and TOP–S solutions were prepared by dilution. All chemicals were used as received. Temporary tattoo transfer paper were purchased from Yuanteng.

Procedure for Synthesis of Green-Emitting QDs (G-CdSe/ZnS QDs): The synthesis recipe is a modified version of a previously reported method.[54] CdO (0.18 mmol), 3.14 mmol $Zn(OAc)_2$, and 7 mL OA were placed in a 10 mL three-neck round bottom flask and degassed for 1 h at 150 °C. After introducing 15 mL ODE, the temperature was raised to 290 °C under inert gas atmosphere. TOP solution (2 mL) containing 1.5 mmol Se and 2.5 mmol S swiftly injected at this temperature. After waiting 10 min 0.7 M ODE-S solution injected at 310 °C. After 12 min, solution of 0.4 mmol $Zn(OAc)_2$•$2H_2O$, 3.5 mL ODE and 1 mL OA was added dropwise. At the end of 10 min the reaction was cooled to room temperature. Resultant QDs were precipitated by centrifugation at 5000 rpm for 10 min with the addition of excess ethanol and redispersed in n-hexane.

Procedure for Synthesis of Blue-Emitting QDs (B-CdZnS/ZnS QDs): The synthesis recipe is a modified version of a previously reported method.[55] A 100 mL three-neck round-bottom flask containing 1 mmol of CdO, 10 mmol of $Zn(OAc)_2$, and 7 mL of OA was held at 130 °C under vacuum for 60 min. Then, 15 mL of ODE was added to the system under nitrogen flow and kept under vacuum for 30 min at 90 °C. The temperature was then raised to 310 °C in an inert gas environment. At this temperature, 1.45 mmol S dissolved in 2.40 mL of ODE was swiftly injected into the reaction for the formation and growth of the core.

After waiting for 15 min, the shell was formed by injecting a solution of 4 mmol S in 5 mL of OA into the system with a syringe pump at a rate of 0.8 mL min^{-1}. The reaction was kept at this temperature for 3 h to allow the formation of a thick shell. Resultant QDs were precipitated by centrifugation at 9000 rpm for 20 min with the addition of excess acetone and redispersed in n-hexane.

Procedure for Synthesis of Red-Emitting Dot-in-Rod QDiRs (R-CdSe/CdS QDiRs)—Synthesis of CdSe QDs: Core CdSe QDs were synthesis by following procedure: 52 mg (0.4 mmols) of CdO, 1.82 g (6.4 mmols) of stearic acid, and 4 g of squalane were added to a 50 mL round-bottom flask and evacuated at 100 °C before being back filled with Argon. Cd-stearate was formed by heating to 250 °C, and upon turning clear 1.8 mL of TOP was added. This solution was further heated to 380 °C, at which point the heating mantle was removed, 0.2 mL of 2 M TOP-Se was added swiftly, and the flask was immediately cooled to 80 °C using an air jet. The resulting CdSe quantum dots were purified by addition of excess acetone followed by centrifugation at 6000 rpm for one minute. Acetone rinsing was repeated twice to remove residual liquid organic compounds, and the pellet was resuspended in hexane before centrifuging again. The supernatant containing quantum dots in hexane was stored in a refrigerator for future use, and the pellet containing residual solid organic compounds was discarded. The concentration of QDs was determined from absorbance.

Procedure for Synthesis of Red-Emitting Dot-in-Rod QDiRs (R-CdSe/CdS QDiRs)—Synthesis of CdSe/CdS QDiRs QD: Synthesis of dot-in-rods was based on a previously published procedure.[56] CdSe (50 nmols) QDs in hexane were transferred to a vial inside a glovebox, and a solution containing 0.5 mmols S dissolved in 3 mL TOP was added. Hexane were evaporated by stirring the solution at 100 °C for 30 min. Separately, 128 mg (1 mmol) of CdO, 334 mg (1 mmol) of ODPA, 166 mg (1 mmol) of HPA, and 4 g of squalane were added to a 50 mL round-bottom flask and evacuated at 100 °C before being back filled with Argon. Cd-phosphonate was formed by heating to 380 °C. Upon turning clear, the solution was cooled to 350 °C, and the solution of CdSe QDs dissolved in TOP–S was added swiftly. The CdS rod was grown by annealing at 350 °C for 20 min. The resulting product was then cooled to 80 °C using an air jet, and purified using ethanol, acetone, and toluene. The pellet was resuspended in hexane and centrifuged to remove insoluble organic materials. The supernatant containing two-color heterojunction nanorods in hexane was stored in a refrigerator for further use.

Fabrication and Transferring of Unclonable Features on Tattoo Paper by Electrospraying: Powdered QDs and QDiRs were weighed and their content in chloroform was kept constant at 10 mg mL^{-1}. The preceding dispersion was then added with PMMA at a concentration of 10% w/w, and the solutions were stirred with a magnetic stirrer until the polymer was fully dissolved. Then, the polymer solutions were electrosprayed onto the surface of the transfer side of the tattoo papers (and silicon wafers for the characterization purpose) using a commercial electrospinner (Holmarc HO-NFES-040). The solutions were placed in a 2.5 mL syringe fitted with a blunt end 18-gauge metallic needle. The syringe was placed in a horizontal configuration against a grounded collector consisting of an aluminum cylinder. Tattoo paper were cut into small pieces about with a size of 10 × 10 mm^2 and taped from back side to the aluminum collector. The tip to the substrate distance, applied potential and flow rate were kept constant as 15 cm, 15 kV, and 1 mL h^{-1} respectively. Electrospraying for around 10 s can directly produce TQPUFs patterns with a single kind of photoluminescent solution, whereas electrospraying in sequencing of solutions on the same surface can produce TQPUFs with several subtypes. Electrosprayed tattoo papers was then translated upside down onto surface of silicon wafer or the desired object. Then the tattoo sheets' backing paper is peeled off after being wetted and gently rubbed to adhere a thin transfer layer.

Characterization: An upright research microscope (ZEISS Axio Imager 2) was used to acquire optical and fluorescence images of the samples. This microscope used a 100 W mercury arc lamb (HBO 100) as the multispectral light source. The fluorescence images of PUFs were acquired by using different excitation and emission filters. For practical image acquisition, a handheld fluorescence microscope (Dino Lite AM7115MT-FUW) with a UV light source of 375 nm was used. The morphology of the electrosprayed features was imaged by using scanning electron microscopy (SEM) (Zeiss EVO LS10) operated at 25 kV and FE-SEM (Zeiss GEMINI) operated at 2 kV. The images taken from SEM, optical bright field, and fluorescence microscopy were analyzed by an image analysis program (ImageJ) to determine the statistical distribution of the size of obtained features. For optical characterization, semiconductor nanocrystals were added to quartz cuvettes with 1 cm path length and diluted in toluene. Absorption was measured using an Agilent 8453 photodiode array spectrometer. PL and PLE spectra were acquired using a HORIBA Jobin Yvon FluoroMax-3 fluorometer. PLQY measurements were carried out with Hamamatsu C11347 absolute PL quantum yield spectrometer. For electron microscopy, nanocrystals were diluted in toluene and drop-cast on amorphous carbon TEM grids. Bright field micrographs were captured using a JEOL 2010 LaB6 TEM at 200 kV.

Extraction of PUF Keys and Calculation of PUF Merits: The binary keys and PUF parameters were acquired using MATLAB software. Briefly, original fluorescence images were binarized separately depending on emission color. Afterward, 16 × 16 or 8 × 8 bit long keys were generated by reducing the size of the original images (for process steps and description, see the Supporting Information and Table S1, Supporting Information). Emission channel dependent extracted keys were then used to calculate uniformity, uniqueness, randomness, and reliability using the equations given in the Supporting Information.

Direct Authentication by Future Detection Algorithms: Tattoo-like multicolor PUFs were verified using an image feature detection algorithm of ORB (Oriented FAST and Rotated BRIEF). The detectORBFeatures function was used for the implementation. Pairwise comparison of the color and the most similar points and features revealed by the algorithms in both images determined the matching between the captured fluorescence image and the database image. With a threshold of 1000, we only considered features and points that were quite close. The initial phase involved the use of ORB to extract the images' characteristics. The second phase involved using a closest neighbor-based approach to match the features extracted from the images. The random sample consensus technique was used in the third stage to clean up the mismatches that occurred during the key point matching in order to calculate the percentile and mean similarity. Identifying and verifying image characteristics and their locations was the fourth stage. An individual recognition score was determined by the percentage of feature points that were correctly matched relative to the total number of feature points.

Stability Tests: Fluorescence stability was evaluated by capturing 100 images of the sample from the same location every 2 min. Similarly, fluorescence images were acquired from the same region of the sample exposed to heating for up to 6 days on a hot plate maintained at a constant temperature of 70 °C to test the emission stability against heat. Time-dependent fluorescence stability of each emission channel against light and heat stressors was shown by analyzing the reduction in the intensity in captured fluorescence microscopy images using the ZEN Blue Lite software.

Supporting Information

Supporting Information is available from the Wiley Online Library or from the author.

Acknowledgements

This work was supported by The Scientific and Technological Research Council of Turkey (TUBITAK) under grant no. 119F384. MS acknowledges support from US National Science Foundation (NSF) under grant no. 2132538.

Conflict of Interest

The authors declare no conflict of interest.

Data Availability Statement

The data that support the findings of this study are available from the corresponding author upon reasonable request.

Keywords

electrospraying, physically unclonable function, polymers, security labels, semiconductor nanocrystals

Received: October 12, 2023
Revised: November 8, 2023
Published online: December 7, 2023

[1] R. Pappu, B. Recht, J. Taylor, N. Gershenfeld, *Science* **2002**, *297*, 2026.
[2] T. Mcgrath, I. E. Bagci, Z. M. Wang, U. Roedig, R. J. Young, *Appl. Phys. Rev.* **2019**, *6*, 011303.
[3] Y. Gao, S. F. Al-Sarawi, D. Abbott, *Nat. Electron.* **2020**, *32*, 81.
[4] N. Kayaci, R. Ozdemir, M. Kalay, N. B. Kiremitler, H. Usta, M. S. Onses, *Adv. Funct. Mater.* **2022**, *32*, 2108675.
[5] H. Im, J. Yoon, J. Choi, J. Kim, S. Baek, D. H. Park, W. Park, S. Kim, *Adv. Mater.* **2021**, *33*, 2102542.
[6] J. Feng, W. Wen, X. Wei, X. Jiang, M. Cao, X. Wang, X. Zhang, L. Jiang, Y. Wu, *Adv. Mater.* **2019**, *31*, 1807880.
[7] J. Wu, J. Li, X. Liu, L. Gong, J. Chen, Z. Tang, W. Lin, Y. Mu, X. Lin, W. Hong, G. Yi, X. Chen, *ACS Appl. Mater. Interfaces* **2022**, *14*, 2369.
[8] J. Wu, X. Liu, X. Liu, Z. Tang, Z. Huang, W. Lin, X. Lin, G. Yi, *Chem. Eng. J.* **2022**, *439*, 135601.
[9] T. Zhang, Z. Shu, L. Zhang, Y. Chen, Z. Feng, Y. Hu, F. Huang, P. Wang, D. Li, Y. Yao, S. Sun, H. Duan, *Adv. Mater. Technol.* **2021**, *6*, 2001073.
[10] J. Yan, G. Pan, W. Lin, Z. Tang, J. Zhang, J. Li, W. Li, X. Lin, H. Luo, G. Yi, *Chem. Eng. J.* **2023**, *451*, 138922.
[11] S. Qiang, K. Yuan, Y. Cheng, G. Long, W. Zhang, X. Lin, X. Chai, X. Fang, T. Ding, *J. Mater. Chem. C* **2023**, *11*, 7076.
[12] M. R. Carro-Temboury, R. Arppe, T. Vosch, T. J. Sørensen, *Sci. Adv.* **2018**, *4*, e1701384.
[13] Y. Lu, H. Cheng, G.-C. Li, F. Han, C. Jiang, T. W. Lo, D. Lei, P. S. Francis, Y. Zheng, *Adv. Funct. Mater.* **2022**, *32*, 2201372.
[14] J. Wang, Q. Zhang, R. Chen, J. Li, J. Wang, G. Hu, M. Cui, X. Jiang, B. Song, Y. He, *Nano Today* **2021**, *41*, 101324.
[15] J. Kim, J. M. Yun, J. Jung, H. Song, J.-B. Kim, H. Ihee, *Nanotechnology* **2014**, *25*, 155303.
[16] Y. Zheng, C. Jiang, S. H. Ng, Y. Lu, F. Han, U. Bach, J. J. Gooding, *Adv. Mater.* **2016**, *28*, 2330.
[17] J. W. Leem, M. S. Kim, S. H. Choi, S.-R. Kim, S.-W. Kim, Y. M. Song, R. J. Young, Y. L. Kim, *Nat. Commun.* **2020**, *11*, 328.
[18] M. S. Kim, G. J. Lee, J. W. Leem, S. Choi, Y. L. Kim, Y. M. Song, *Nat. Commun.* **2022**, *13*, 1.
[19] J. Park, J. W. Leem, Z. Ku, J. O. Kim, W. C. Chegal, S.-W. Kang, Y. L. Kim, *ACS Appl. Nano Mater.* **2021**, *4*, 2076.

[20] Y. Liu, F. Han, F. Li, Y. Zhao, M. Chen, Z. Xu, X. Zheng, H. Hu, J. Yao, T. Guo, W. Lin, Y. Zheng, B. You, P. Liu, Y. Li, L. Qian, *Nat. Commun.* **2019**, *10*, 1.
[21] X. Zheng, Y. Zhu, Y. Liu, L. Zhou, Z. Xu, C. Feng, C. Zheng, Y. Zheng, J. Bai, K. Yang, D. Zhu, J. Yao, H. Hu, Y. Zheng, T. Guo, F. Li, *ACS Appl. Mater. Interfaces* **2021**, *13*, 15701.
[22] O. Ivanova, A. Elliott, T. Campbell, C. B. Williams, *Addit. Manuf.* **2014**, *1-4*, 24.
[23] N. M. Abdelazim, M. J. Fong, T. McGrath, C. S. Woodhead, F. Al-Saymari, I. E. Bagci, A. T. Jones, X. Wang, R. J. Young, *Sci. Reports.* **2021**, *11*, 1.
[24] F. Chen, Q. Li, M. Li, F. Huang, H. Zhang, J. Kang, P. Wang, *Chem. Eng. J.* **2021**, *411*, 128350.
[25] L. Zhao, X. Chen, J. Fu, C. Xue, M. Zhang, W. Wen, J. Wu, *Appl. Surf. Sci.* **2021**, *567*, 150827.
[26] P. Kumar, K. Nagpal, B. K. Gupta, *ACS Appl. Mater. Interfaces* **2017**, *9*, 14301.
[27] T. Ritacco, G. E. Lio, X. Xu, A. Broussier, A. Issa, M. Giocondo, R. Bachelot, S. Blaize, C. Couteau, S. Jradi, *ACS Appl. Nano Mater.* **2021**, *4*, 6916.
[28] A. Esidir, N. B. Kiremitler, M. Kalay, A. Basturk, M. S. Onses, *ACS Appl Polym Mater* **2022**, *4*, 5952.
[29] G. Taylor, *Proc Math Phys Eng Sci* **1969**, *313*, 453.
[30] A. M. Gañán-Calvo, J. M. López-Herrera, M. A. Herrada, A. Ramos, J. M. Montanero, *J. Aerosol Sci.* **2018**, *125*, 32.
[31] E. Bodnár, J. Grifoll, J. Rosell-Llompart, *J. Aerosol Sci.* **2018**, *125*, 93.
[32] L. Rayleigh, **2009**, *14*, 184.
[33] H. Brandenberger, D. Nüssli, V. Piëch, F. Widmer, *J Electrostat* **1999**, *45*, 227.
[34] A. Jaworek, A. T. Sobczyk, *J Electrostat* **2008**, *66*, 197.
[35] F. Sahin, S. Pekdemir, M. Sakir, Z. Gozutok, M. S. Onses, *Adv. Mater. Interfaces* **2022**, *9*, 2200048.
[36] G. E. Bonacchini, C. Bossio, F. Greco, V. Mattoli, Y.-H. Kim, G. Lanzani, M. Caironi, *Adv. Mater.* **2018**, *30*, 1706091.
[37] J. Barsotti, A. G. Rapidis, I. Hirata, F. Greco, F. Cacialli, V. Mattoli, *Adv. Electron. Mater.* **2021**, *7*, 2001145.
[38] M. J. Smith, C. H. Lin, S. Yu, V. V. Tsukruk, *Adv. Opt. Mater.* **2019**, *7*, 1801072.
[39] T. Ma, T. Li, L. Zhou, X. Ma, J. Yin, X. Jiang, *Nat. Commun.* **2020**, *11*, 1
[40] P. Martinez, I. Papagiannouli, D. Descamps, S. Petit, J. Marthelot, A. Lévy, B. Fabre, J.-B. Dory, N. Bernier, J.-Y. Raty, P. Noé, J. Gaudin, *Adv. Mater.* **2020**, *32*, 2003032.
[41] G. Chen, Y. Weng, W. Wang, D. Hong, L. Zhou, X. Zhou, C. Wu, Y. Zhang, Q. Yan, J. Yao, T. Guo, *ACS Appl. Mater. Interfaces* **2021**, *13*, 27548.
[42] L. Jing, Q. Xie, H. Li, K. Li, H. Yang, P. L. P. Ng, S. Li, Y. Li, E. H. T. Teo, X. Wang, P.-Y. Chen, *Matter* **2020**, *3*, 2160.
[43] A. Maiti, V. Gunreddy, P. Schaumont, in *Embed. Syst. Des. with FPGAs*, Springer, New York, **2013**, pp. 245–267.
[44] A. Rukhin, J. Soto, J. Nechvatal, M. Smid, E. Barker, S. Leigh, M. Levenson, M. Vangel, D. Banks, A. Heckert, J. Dray, S. Vo, n.d., https://doi.org/10.6028/NIST.SP.800-22r1a.
[45] N. Torun, I. Torun, M. Sakir, M. Kalay, M. S. Onses, *ACS Appl. Mater. Interfaces* **2021**, *13*, 11247.
[46] E. Rublee, V. Rabaud, K. Konolige, G. Bradski, presented at *Proc. IEEE Int. Conf. Computer Vision*, Barcelona, Spain, **2011**, 2564.
[47] M. Calonder, V. Lepetit, C. Strecha, P. Fua, *Lect. Notes Comput. Sci. (including Subser. Lect. Notes Artif. Intell. Lect. Notes Bioinformatics)* **2010**, *6314 LNCS*, 778.
[48] M. Sakir, N. Torun, N. Kayaci, I. Torun, M. Kalay, M. S. Onses, *Mater Today Chem* **2023**, *29*, 101423.
[49] A. Esidir, N. Kayaci, N. B. Kiremitler, M. Kalay, F. Sahin, G. Sezer, M. Kaya, M. S. Onses, *ACS Appl. Mater. Interfaces* **2023**, *15*, 41373.
[50] S. Lee, S. Pekdemir, N. Kayaci, M. Kalay, M. S. Onses, J. Ye, *ACS Appl. Mater. Interfaces* **2023**, *15*, 33878.
[51] S. A. K. Tareen, Z. Saleem, *2018 Int. Conf. Comput. Math. Eng. Technol. Inven. Innov. Integr. Socioecon. Dev. iCoMET 2018 – Proc.*, **2018**, 1.
[52] Y. Lu, H. Chen, H. Cheng, H. Qiu, C. Jiang, Y. Zheng, *ACS Appl. Nano Mater.* **2022**, *5*, 9298.
[53] F. Han, Y. Liu, F. Li, Y. Lu, H. Cheng, Y. Lin, T. Zhao, S. H. Ng, U. Bach, Y. Zheng, *J. Mater. Chem. C* **2019**, *7*, 13040.
[54] K.-H. Lee, J.-H. Lee, H.-D. Kang, B. Park, Y. Kwon, H. Ko, C. Lee, J. Lee, H. Yang, *ACS Nano* **2014**, *8*, 4893.
[55] K.-H. Lee, J.-H. Lee, W.-S. Song, H. Ko, C. Lee, J.-H. Lee, H. Yang, *ACS Nano* **2013**, *7*, 7295.
[56] L. Carbone, C. Nobile, M. De Giorgi, F. D. Sala, G. Morello, P. Pompa, M. Hytch, E. Snoeck, A. Fiore, I. R. Franchini, M. Nadasan, A. F. Silvestre, L. Chiodo, S. Kudera, R. Cingolani, R. Krahne, L. Manna, *Nano Lett.* **2007**, *7*, 2942.